Nanostructuring Ferroelectrics via Focused Ion Beam Methodologies

Burns, S. R., Gregg, J. M., & Nagarajan, V. (2016). Nanostructuring Ferroelectrics via Focused Ion Beam Methodologies. Advanced Functional Materials. DOI: 10.1002/adfm.201603812

Published in:
Advanced Functional Materials

Document Version:
Peer reviewed version

DOI: 10.1002/
Article type: Review

Title: Nanostructuring Ferroelectrics via Focused Ion Beam Methodologies

*Stuart R. Burns, J. Marty Gregg and Valanoor Nagarajan**

S.R. Burns, Prof. V. Nagarajan
School of Materials Science and Engineering, University of New South Wales, Sydney 2052, Australia
E-mail: nagarajan@unsw.edu.au
Prof. J. Marty Gregg
Centre for Nanostructured Media, School of Mathematics and Physics, Queen's University Belfast, University Road, Belfast BT7 1NN, UK

Keywords: focused-ion-beam, ferroelectrics, piezoresponse, exotic domain states, domain wall mobility.

As we reach the physical limit of Moore's law and silicon based electronics, alternative schemes for memory and sensor devices are being proposed on a regular basis. The properties of ferroelectric materials on the nanoscale is key to developing device applications of this intriguing material class, and has been readily pursued in recent times. One of the most significant techniques with which nanostructuring is achieved is the focused-ion-beam (FIB) microscope. Alongside nanoscale characterization obtained from piezoresponse force microscopy, the FIB has become a powerful tool in the search for first principles understanding of the ferroelectric phenomena. This review explores a brief history of the relationship between the FIB and ferroelectrics, the fascinating properties it has unveiled, and some alternative nanostructuring techniques.

1. Introduction

Over recent times, there has been a significant increase in the attention given to researching nanoscale ferroelectric and multiferroic materials. Analogous to ferromagnets and their magnetisation, ferroelectrics have a spontaneous order parameter which exists in at least two stable states and can be switched between them through the application of an external electric field.[1] This polarisation can be actively controlled through the direct piezoelectric and converse piezoelectric effects, in which a mechanical stress is used to generate a dipolar moment in the unit cell, and conversely where an electric field causes an induced strain on the lattice. Such 'smart material' properties are commonly used for sensor, actuator and memory applications, [2, 3] but on approaching the nanoscale, the difficulty in scaling certain functional properties becomes clear.[4-6] Size reduction in ferroelectrics has revealed enhanced or drastically changed properties in numerous cases,[7-10] and vertical scaling through thin film growth provides a plethora of opportunities in which the functional features can be modified.[11-13] On the other hand, as the dimensionality of the material system is reduced, our understanding decreases. These effects are not yet fully explored or understood, and require techniques to fabricate ferroelectric nanostructures from which we can develop an advanced platform of knowledge based on first principles for this material class.

For instance, the ferroic materials system bismuth ferrite (BFO) has sparked an explosion of studies on its fascinating multiferroic properties.[14] With a tetragonal-like phase in ultra-thin films (T-phase) which progressively relaxes upon the growth of additional film layers (to R-phase, as it is in bulk), there is a large interest in the areas of film which show a mixed-phase configuration.[15] In these areas, it was noted that ferroelectric pinning and relaxation would be present, drastically changing the functional properties in the region.[7] The effect of substrate induced strain on BFO was also investigated by Johann et al., whereby four different substrates were used as hosts for BFO thin films, with a range of strains from -1.4% to +0.75%. Through

a full collection of characterisation experiments, the group showed that strain caused the rotation of the unit cell, suppression of certain domain variants, but consistent switching behaviour across all substrates.[13] The complexities of the structural phases of BFO is complemented by the enhanced functional properties in the mixed phase, the most notable of which is the ferromagnetic component.[12] Therefore the complete understanding of such a system on the nanoscale is key if the material is to be utilised for device applications.

One instrument that has made possible the synthesis of ferroelectric nanostructures and the fabrication of complete devices is the focused-ion-beam (FIB) microscope. An example of a device partially fabricated through focused-ion-beam processing is given in **Figure 1**. Based on the BFO system, this structure shown in the schematic consists of a multiferroic layer (which simultaneously exhibits both ferroelectric and antiferromagnetic orders) and ferromagnetic layer coupled together at a common interface – this is a proof-of-principle magnetoelectric coupling memory device.[16] Upon switching of the ferroelectric order via an electric field, the coupling ferromagnetic plane also switches. Magnetoelectric coupling, in which a magnetic field is capable of switching an electric polarisation and similarly a magnetic spin can be switched through an electric field, is a phenomena which holds a lot of promise for applications.[17-20] More complex features of the coupling mechanisms in several multiferroics have also become the catalyst for the emerging field of magnonics.[21]

To illustrate the undeniable impact of FIB processing in ferroelectric and multiferroics research, a brief timeline of important milestones in the field is shown in **Figure 2**. This review gives a brief overview of the nanostructuring ferroelectrics in recent years, with a large portion dedicated to discussing the use of the focused-ion-beam.

2. Basic Principles of FIB Instruments

Ions are extracted from a liquid metal ion source and are accelerated through a column of focusing lenses and apertures (to energies of keV magnitude) and into a vacuum chamber. The beam is incident on a sample placed on a stage at a focus to 0.1μm or smaller. The apertures in the column set the diameter and current of the beam incident to the sample surface – low current beams of around 30pA are commonly used for rastor imaging through detecting the backscattered electrons created from the ion-matter interaction.[22] Beam currents of the order of nA and higher are used for sputtering away material in the sample in predefined patterns set by the user.[23] Another FIB capability commonly used in material sciences is local deposition of metals through chemical vapour deposition. The metals commonly available for deposition in commercial FIB systems are platinum (Pt) and tungsten (W).[24]

The physics of ion-matter interactions has been well understood for decades.[25] The potential for lithography, patterning, sputtering and imaging in a single instrument was inspiration for the first attempt to focus a beam of ions for developing integrated circuits on the micron scale in 1973.[26] Commercially available FIB systems are typically based on gallium ions, although several other liquid metal sources can be used (such as Au, Si, Be, B, As, P and others).[25] Gallium (Ga^+) is routinely used because of its low melting temperature, low volatility and low vapour pressure.[22] The most common applications of the FIB are fabricating thin lamellar platelets for transmission electron microscopy (TEM) and other structural investigations, fabricating nanostructures or holes, imaging (although scanning electron microscopy (SEM) is a common alternative as it has a higher resolution and is less invasive and damaging to the sample surface), and microfabrication and repair of circuits through metal deposition.[27, 28] Stencil masks, novel capacitor geometries and proof-of-concept devices can be fabricated due to the flexible imaging and patterning available on the micron/submicron scale.

A significant drawback to the instrument is the slow speed at which milling and patterning occurs, especially for larger structures.[24] Despite the versatility of the instrument, problems arise at the nanoscale due to damage induced by the incident ions displacing atoms in the top few layers of the sample surface. Over time methodologies and techniques have been developed to avoid this inconvenience, as discussed in the next section.

3. Initial Nanostructuring and Characterization of Ferroelectrics

3.1 Setting the Stage for FIB Nanostructuring

As far back as 1998, nanostructuring ferroelectrics was investigated with the long term aim of establishing ferroelectric memories. Alexe et al. created self-assembled capacitor arrays via pulsed laser deposition (PLD).[6] These heterostructures were composed of bismuth titanate (BiT), lanthanum strontium copper oxide (LSCO) and yttria-stabilized zirconia (YSZ) grown on silicon substrates. The structures were of the order of 150-500nm in separation, with lateral dimensions of 125-200nm, which is 50 times smaller than any ferroelectric nanostructures previously fabricated.[29, 30] Despite showing a very lossy hysteresis loop, similar to misidentified ferroelectric materials,[31] the ferroelectric properties were comparable to larger structures made previously from the same material, with a remanent polarization of 4μC/cm^2. These cells were successfully switched in a follow-up investigation[9] – however, through these piezoresponse force microscope (PFM) switching experiments, it was noticed that not all of the structures were ferroelectric. This could have been due to the inhomogeneity across the film or due to the nanostructuring technique. In the latter case, it should be noted that the self-assembly of nanocrystals (by virtue of its instinctive nature) has little to no active control on spatial location in comparison to the FIB.

In 2001, Alexe et al. created nanocapacitors of PZT patterned on Nb-doped STO, through electron-beam lithography, which demonstrated a very significant negative imprint in its hysteretic behaviour.[10] These structures were created at lateral dimensions of around 100nm via electron beam direct writing, in which metalorganic precursors are used to induced chemical reactions in the regions which are exposed to a large electron dose,[32] before being switched with a scanning probe in piezoresponse force microscope mode in order to obtain hysteresis curves.[33]

3.2 Eliminating Ga^+ Induced Damage

The issue of structural damage induced on ferroelectrics by Ga^+ implantation is well documented;[34-36] it is widely agreed that a damaged layer of dielectric material is created due to gallium implantation which is detrimental to the ferroelectric properties of the bulk material beneath the amorphous layer. Annealing is commonly the first attempted recovery procedure used to recrystallise the damaged layer which is thought to be around 10-20nm thick. In a reported recovery process, Schilling et al. highlight the loss of clear symmetric hysteresis curves and poor retention of the switched state caused by gallium damage.[37] Their work demonstrated that annealing alone was not sufficient to fully recover the surface layer of BTO lamella. The lamellar surface was found to become coated in a layer of thin platelets which, after imaging under SEM and TEM, they concluded to be gallium oxide. These platelets were reduced in number through annealing in vacuum instead of conventional air furnaces, and a plasma cleaning process of 30 mins was sufficient enough to completely remove the gallium oxide. In an attempt to prevent any damage during FIB processing, Hambe coated a PZT wafer with electron-beam photoresist as a protective layer.[38] Alongside a dilute acid etching to remove the photoresist and recrystallise the surface if required, this proved successful in preserving the ferroelectric properties of the wafer.

Inspired by AAO masks and other stencil shadow masking techniques,[39, 40] in a study aimed at avoiding any FIB damage, Morelli and co-workers in Halle used a protective layer of Al dots, evaporated through a hard stencil mask, on a thin film of BFO.[41-43] The area containing the array of Al dots was milled by FIB with very low beam currents in order to minimize implantation. Following this, a chemical etch with 10% diluted potassium hydroxide was used to remove any remaining Al. A schematic of the procedure is presented in **Figure 3**. Aluminium was chosen for the protective caps as it was easily removed post-milling and the gallium ions had a very short stopping distance in the material. The resulting sample contained

an array of almost free-standing BFO nanoislands of 250nm diameter with ferroelectric properties similar to the unstructured thin film. PFM scanning was successful in switching polarization in the island, with good retention. However, the islands did exhibit ferroelectric loops with significant imprint, and re-deposition of the milled BFO material and damage at the island edge was problematic and unavoidable.

As a response to the 'dead layer' debate, (which concerns whether or not the interface between electrodes and ferroelectric material is dielectric and how it acts as a capacitance layer),[44] Saad et al. investigated the dielectric response of free-standing BTO lamellar capacitors created by focused-ion-beam milling.[45] They observed Curie-Weiss behaviour, and no dielectric peak broadening or shifts in temperature, indicating a first order phase transformation, in contrast with previous studies.[44, 46-48] This work was further developed by Chang et al. several years later.[49] This study further improved Saad's investigations by removing the lamella from the host bulk material and placing them on a platinised magnesium oxide (MgO) substrate and annealed to verify the effect of scaling on the dielectric response. In order to validate atomistic simulations concerning 'dead layer' interfaces,[50] additional experiments on STO lamella were carried out as a comparative investigation.[51] This study confirmed that 'dead layers' can be engineering out of dielectric-metal interfaces by annealing procedures.

Rémiens et al. created PZT nanostructures from two variations of thin film – one film was grown as an amorphous layer, the other as crystalline.[52] Both were nanostructured via focused ion beam and annealed to crystallize and recrystallize the films, respectively. Amorphous films that were milled prior to crystallization showed a piezoresponse closer to bulk than that of the other films (crystallized, milled and recrystallized). Two example nanocapacitors imaged under an SEM are shown in **Figure 4**, with amorphous and crystalline structures shown on the top and bottom of the figure respectively.

In a similar investigation, Hong and colleagues carried out an investigation into the lapse of piezoelectric properties when BFO is cut into both square and round nanocapacitors.[53] In capacitors of lateral dimensions of approximately 500nm, SEM, XRD (x-ray diffraction) and PFM were utilised to characterize both morphologies. Square structures were found to show a single domain variant alongside a strong voltage imprint in the hysteresis curve. In the round capacitors, seven domain variants were visible and the hysteresis curves showed no obvious imprint. The strain gradients in these nanostructures were later investigated, with the results indicating a significant internal mechanical strain, replacing the strain imposed via the substrate clamping prior to FIB patterning.[54] In a follow-up study, the same group highlighted one aspect of the research into FIB processed ferroelectrics that cannot be understated and must be correctly utilised – piezoresponse force microscopy. Despite this technique being well established in present ferroelectrics research efforts, it has not been without problems. The role of the PFM probe buckling during scanning the nanostructures was seen to cause a coupling effect of vertical and lateral piezoresponse signals.[55] This was addressed by varying the position of the laser incident on the top of the cantilever – at the free end of the probe the coupling effect was most dominant. The coupling was minimized at around 60% of the length of the cantilever from the pivot.

3.3 Characterizing Nanostructured Ferroelectrics

Early reports found that FIB milled nanocapacitors suffered from significant degradation in their functional response. However, once the findings on repairing damage were widely known, the method was quickly exploited to create nanostructures in innovative geometries, resulting in many cases of intriguing new phenomena being observed. Early studies of the switching and functional properties of ion milled capacitors was carried out on strontium bismuth tantalate, $SrBi_2Ta_2O_9$ (SBT) by Amanuma and Kunio.[29] The capacitor arrays were comprised of several ferroelectric, dielectric and electrode layers, resulting in a thickness of

2μm prior to milling. A comparison of hysteresis loops for 1.7μm^2 and 10μm^2 capacitor areas was made for a range of input voltages. It was found that at 5V input and higher the curves were extremely similar. However, below this voltage there was noticeable difference between the two capacitors in both hysteresis shape and remanent polarization. The distortion of the 1.7μm^2 capacitor was recovered by applying a 5V input before taking a hysteresis curve at 3V input. This higher voltage was thought to release pinned domain walls and eliminate an internal field in the film. Switching responses were found to be stable down to a driving voltage of 2V. When applying only 1V, the retention of switched charges was found to decrease significantly – this was identified as an obstacle to non-volatile ferroelectric memories which operate at low-voltages. Uchida et al.[30] found that SBT and niobium-doped SBT capacitors constructed from both "top-down" and "bottom-up" procedures gave similarly high retention for 2μm^2 arrays.

Stanishevsky et al. carried out similar procedures with niobium-doped (Nb) PZT-based capacitors.[56] They found that hysteresis curves were attainable down to the 1μm^2 scale, despite significant degradation. Capacitors of 0.017μm^2 were also fabricated successfully without depositing a sacrificial or protective layer on the sample surface. Ganpule's work with scaling properties of ferroelectrics via the focused ion beam created capacitor structures based on Nb-doped PZT[57] and SBT[58] thin films. Ferroelectric properties were exhibited in capacitors of ~0.1μm^2 lateral size in both cases. **Figure 5** shows such capacitors imaged via scanning ion beam.

Simultaneously and independently, both the groups at EPFL and Maryland discovered enhancement in the piezo properties of PZT nanocapacitors.[59, 60] In structures of submicron size, unclamping of the film occurred. This resulted in a significant increase of the piezoelectric response in capacitors of 0.3μm [59] and 0.5μm [60] lateral dimensions. A range of nanocapacitor sizes imaged under SEM are shown in **Figure 6**. For these elements, no distortion of the ferroelectric hysteresis was apparent – this was explained through the abundance of *a* domains

present in the nanostructured samples.[59] In the Maryland study, a range of PZT compositions were analysed. Hard ferroelectric capacitors ($PbZr_{0.2}Ti_{0.8}O_3$) showed a field dependence of d_{33} which followed thermodynamic theory. This is highlighted in **Figure 7**, where the normalized dielectric response is plotted against the applied electric field – the continuous film is shown to have a slower response than the unclamped island structure.[61] However, the response of d_{33} for soft ferroelectrics approaching the morphotropic phase boundary ($PbZr_{0.5}Ti_{0.5}O_3$) did not match the predicted piezoelectric response under an applied field. **Figure 8** is the hysteresis loops for the soft (top) and hard (bottom) ferroelectric compositions. For the soft compositions, the drop between predicted (solid black line) and measured (black squares) response is obvious. The zero-field piezoconstant across the range of compositions was, however, well matched to theory. These results are contrasted by the work of Alexe et al. as discussed in section 3.1.[10]

4. Domain Engineering and Manipulation via FIB Nanostructuring

4.1. Self-assembled Exotic Domain States

Significant investigations of morphological control of domain structures were carried out and reported in a series of publications by Schilling et al. on $BaTiO_3$ (BTO). The research started with focused ion beam milling to create lamellar platelets from bulk single crystals as described previously. Lamellae of varying thicknesses imaged with a scanning transmission electron microscope showed the validity of Kittel's law in the material down to 70nm.[62]

In another of the investigations, the lamellae remained connected to the bulk and the entire sample was tilted *in situ* to mill nanocolumn structures into the platelet face. Upon heating the sample above the Curie temperature and allowing it to cool, the domain structure was imaged under STEM. The constraint caused by the FIB machining lead to an increase the domain number density as the thickness dimensions of the nanocolumn decreased – consistent with observations made by Kittel and others.[63-66] Somewhat unexpectedly, however, the domain periodicity was found to be dependent on only one of the two thickness magnitudes. This relationship was explained by the presence of uncompensated charges on only one set of parallel surfaces. The equilibrium state in the columns was established through competition between the energy associated with the surface charges and that associated with the domain number density.[67]

Further to this relationship between domain periodicity and physical constraint, a study into reorientation of local spontaneous polarization through shape engineering was reported by the group. By modifying the aspect ratio of the nanocolumn dimensions, the surface at which the depolarizing field is evident can be selected. The energy minimization that follows causes half of the domains to reorientate from in-plane to out-of-plane.[68]

Schilling's work into nanodots of BTO is also interesting. STEM (scanning transmission electron microscopy) images of the domain configurations in structures of cross-sectional size

500nm to less than 100nm all showed quadrant packets forming once cycled through the Curie temperature.[69] However, when imaged under PFM (piezoresponse force microscopy) the nanodots displayed flux-closure chains. These contradictory observations were attributed to effect of the TEM sample environment – while in vacuum and under the electron beam the sample is exposed to a radial electric field which causes a charging effect and thus net polarization configurations arise.[70, 71] Upon further PFM imaging the domain structure was shown to be composed of zig-zagging 90° stripe domain bundles appearing as 180° "superdomains". These were suggested to be caused by Landau-Kittel like scaling for dots below critical dimensions, which suggested that their existence was related to depolarizing fields across the nanodot geometries.[72, 73] In a study by McGilly it was shown that these flux-closure and quadrupole configurations did occasionally form in BTO lamella also, but the systems consistently avoided creating point singularity structures, as it was energetically favourable to form complex domain wall patterns with diads or centres of inversion instead.

As with the BTO nanocolumns, the effect of modifying the aspect ratio of dimensions on a nanodot system was explored. It was found that with rectangular cross-sections, the centre point of the quadrant packet migrated further to the shorter edge of the surface. STEM images of this effect are shown in **Figure 9**. This was understood a phase transition described through a Landau free energy expansion in which the off-centering of the structure was modelled as the effective order parameter and the aspect ratio acts analogously to temperature in thermally driven phase transitions.[74]

Of note is a study by McQuaid *et al.* centred on switching BTO lamellae via an applied electric field from a scanning probe tip across a Pt electrode architecture.[75] Once allowing the switched domain states to relax, they were found to also form quadrant structures made up of 90° stripe domain boundaries. In this case however, the structures were consistently comprised of flux-closure polar configurations, as shown in **Figure 10**. This was rationalized to be a result

of the relaxation from a fully polarized monodomain state, which was not applicable to previous searches for these exotic domain states.[72, 76-79] The domain wall kinetics were described as creep processes, similar to that seen in previous studies into oxide ferroelectrics.[80] The study also found that during relaxation the domain kinetics were heavily influenced by depolarizing electric fields and stress fields – but could not rule out the possibility of vortex-vortex interactions playing a secondary role at a scale only visible with improved spatial and time resolutions.[81]

Other ferroelectric materials were also studied in order to find flux-closure loops, the most notable of which are lead zirconate titanate (PZT)[77-79, 82, 83] and bismuth ferrite (BFO).[76, 84] Nanodots of PZT produced through FIB milling were shown to contain closed polarization loops, similar to those seen in ferromagnetic dots.[82] In the analysis of the domain configuration it was assumed that charged domain walls were energetically unfavourable, and therefore flux-closure configurations were the most feasible domain states. A study by Gruverman and co-workers in 2008 established the dependence of vortex configurations in PZT on shape constraints, as they found that upon poling both a square and circular capacitor, only the circular would relax into a vortex configuration.[78] However, research carried out by Ivry[77] seems to indicate that while the structures are size dependant, physical edges are not necessary for nucleation – this would be contrary to suggestions made by Gruverman. For flux-closure structures to be fully identified and analogous to ferromagnetic closed loops, continuous rotation of the order parameter must be present. This was observed by Jia et al. in PZT through TEM imaging.[85] Other notable methods of inducing vortices in PZT nanodots include thin film grown via pulsed laser deposition through AAO stencil masks to create nanoislands in a “bottom-up” methodology, (as discussed in section 5 of this review).[79]

In PZN-12PT (lead zinc niobate – lead titanate), it was observed that mesoscale flux-closure structures where mirrored by nanoscale closed loops embedded within them.[83] These

complex domains were present at the edges of ion milled lamella, and were rationalized by considering the depolarising field in these areas. The fact that both meso- and nanoscale imaging indicated very similar configurations suggests that singularity are both unlikely and unfavourable in complex quadrant domains in ferroelectrics. The same group studied PZN-12PT lamella placed on their sidewalls on Pt-coated MgO carriers.[86] They found that the change in clamping between the lamella placed flat and those placed on their sidewalls caused a variation in domain configurations. Following a heating treatment, those mounted on their sidewalls exhibited irregular domain arrangements similar to relaxor configurations, while those placed flat showed standard typical ferroelectric domains. In 2015, PT films grown on GSO (gadolinium scandium oxide) substrates and imaged under STEM exhibited an array of both clockwise and anticlockwise flux-closure quadrants with extremely large strain gradients (10^9 per meter) around each quadrant core.[87]

BFO thin films were also found to form vortices upon poling by others.[76, 84] In the work carried out by Vasudevan,[76] closure domain arrangements were believed to be caused by defects arising in the centre of the configuration. This defects were induced by the applied electric field of the PFM tip in contact with the surface, which when combined with the inherent ferroelastic walls in the region breaking the symmetry of the system, resulted in a topologically visible closed quadrant loop. Nelson and colleagues fabricated BFO thin films on an insulating substrate (trans-stilbene oxide, TSO), and observed spontaneously formed flux-closure patterns at the locality of the interface. The 109° domain walls which are present in the BFO are incident at the insulator interface – this was thought to be the cause of the polarisation-closure, which exhibited uncharacteristic properties such as mixed Ising-Neel type walls and an enhanced in-plane polarization. Both of these results from the study of BFO indicate the importance of interface and defect physics in multiferroics and device applications.

4.2 Domain Wall Injection and Mobility

The first noticeable example of using FIB nanostructuring to manipulate domain wall dynamics came as a result of previous work from Maryland on the modified piezoelectric coefficient of PZT nanostructures.[60] As the change in dielectric response, d_{33}, was attributed to the change in the ratio of *a* to *c* domains, or 90° and 180° domain walls respectively, further work on these nanoislands was carried out. The new study involved domain mapping with PFM after applying a switching bias with the probe tip.[88] It was shown that the unclamping of the PZT through nanostructuring depinned the 90° domain walls and allowed them to move up to 130nm across the islands. It was also reaffirmed that these walls contributed to the piezoelectric properties of the structures. Shown in **Figure 11** is PFM data from these experiments, highlighting the movement of walls over differing polarities. The next plot, **Figure 12**, shows d_{33} across a range of positive AC voltages, where the red points represent the island and the blue represent the clamped film. The peak in the piezoresponse corresponds to the coercive field for 90° domain walls.[61] Finally, the piezoelectric response (d_{33}) was plotted against the applied pulse width for a clamped film, a 100nm thick unclamped island, and a 1µm thick unclamped island, shown in **Figure 13**. As expected, the clamped film and 100nm thick island both exhibited no increased response across the range of pulses, as neither contain any 90° walls. The 1µm thick film, however, showed an increased d_{33} for longer pulses.[61] This manipulation of ferroelastic domain walls in ferroelectric materials has not been explored any further.

In 2009, with the realisation of domain walls with larger conduction than that of their host materials, further intrigue developed into domain wall nucleation and manipulation.[89] The emergent field of domain wall nanoelectronics[90] inspired a flurry of investigations into the mobility of these interfaces. The following is a brief summary of a series of publications

by the group in Queen's University Belfast and collaborators. In each of these works, FIB processing was used in some way to explore domain wall dynamics.

Beginning with McMillen and McQuaid in 2010, the effect of milling notches and anti-notches into ferroelectric lamella and nanowires was studied. McMillen's study into notches along BTO nanowires generated a counterintuitive result – despite expecting them to cause domain wall pinning, enhanced switching speeds of domains around the locality of the defects were observed.[91] Through finite element field modelling of the patterned wires, the narrower areas of the ferroelectric and the air gap surrounding them were found to exhibit local field enhancement. In the same simulations, the effect of antinotches was questioned – this led to McQuaid's subsequent study of antinotched BTO nanowires.[92] Here, the patterning was found to cause a reduction in the magnitude of the local electric field under bias. However, it was not of the order of magnitude of the field enhancement observed in the notched wires. The difference in domain wall mobility was also more subtle in the antinotched systems. These initial examinations started a programme of 'field-engineering' through FIB patterning.

The next question addressed was whether or not induced size constraints would routinely cause increased switchability in BTO.[93] A comparison of domain nucleation and mobility in single crystal nanorods and lamellar plates showed that unclamping the structure in a lateral direction did encourage switchability. Placed across an inter-electrode arrangement, polar switching in plates was seen to occur through initial domain wall nucleation across electrodes, followed by sidewall growth and secondary nucleation. This seems to indicate why rods were more easily switched – a minimum amount of sidewall migration would be required in these structures.

An equation of motion for superdomain boundaries in BTO lamella was discussed by Sharma et al. in 2013.[94] In-situ PFM imaging of domain dynamics seemed to suggest a ballistic projectile motion of the boundary – initially displaced at a rapid velocity, the boundary

begins to decelerate. However, to suggest that this was due to the domain experiencing a drag would be unphysical. As an alternative explanation, a screening effect from depolarizing fields was suggested to be causing the change in nucleation velocity.

Whyte et al. demonstrated how domain wall injection in potassium titanyl phosphate (KTP) can be controlled.[95] By milling both circular and triangular holes into a lamellar structure, local field enhancement ('hot-spots') and field diminishment ('cold-spots') were induced. By applying a progressively larger bias in these patterned plates, the process of domain wall injection was imaged over time. Finite element modelling accurately predicted how the ferroelectric/air interface affected local field magnitudes in the lamella, as shown in **Figure 14**. Domain wall pairs were successfully injected and they were shown to move preferentially in certain directions due to the shape and location of milled defects. With this in mind, Whyte demonstrated that through both milling holes into KTP lamellae and by patterning antinotches in the Pt electrodes (reducing the inter-electrode gap across the lamella) one can selectively induce domain walls across a capacitor geometry.[96] In this way, specific nucleation can be induced at a known magnitude of applied bias through a PFM probe – this will change the resistance across the capacitor according to the number of nucleated walls, demonstrating an effective memristor proof-of-concept device.

As a combination of the knowledge gained from the publications previously discussed, Whyte developed a ferroelectric domain wall diode.[97] This lamellar structure made up of KTP exhibited a sawtooth morphology and was placed onto a coplanar electrode configuration, as shown in the schematic in **Figure 15**. With the sample initially in a fully switched monodomain state, it was observed that the thickness profile caused domain wall motion to only be possible in one direction; walls could move up the shallow incline but could not move in the opposite direction due to the steep change in gradient at the edge of the 'tooth' – hence this is a domain wall diode proof-of-principle device.

5. Alternatives to FIB Nanostructuring

One nanostructuring concept to receive noticeable attention is the self-assembly of nanopillars in a host matrix material, the most common of which compromises of spinel pillars in perovskite matrices.[98] The first reported case of such a sample structure was in 2004, where via PLD barium titanate ($BaTiO_3$, BTO) was grown with cobalt ferrite ($CoFe_2O_4$, CFO) pillars embedded throughout.[99] The self-assembling CFO columns are epitaxial in both lateral and vertical directions, with a minimum amount of substrate clamping due to diameters of only 20-30nm. There is a strong magnetoelectric coupling present caused by the large surface/volume ratio between the columns and the matrix material, which is apparent when heating the material to the ferroelectric Curie temperature of BTO and observing a change in the net magnetization. Another spinel-perovskite system that was fabricated was CFO-BFO pillar-matrix structures.[100] The magnetisation could be switched upon applying an electric field in these structures which exhibited a magnetoelectric susceptibility of ~$1x10^{-2}$ G cm/V, again credited to the ferroelastic coupling caused by the epitaxial growth in three dimensions. The switching behaviour was later improved upon by applying a weak magnetic field alongside the electrical bias in order to selectively switch specific nanopillars.[101] NFO-BFO (nickel ferrite - bismuth ferrite) nanocomposite films were structurally analysed to confirm the ferroelastic nature of the spinel-perovskite coupling.[102] A thorough study into the crystallography of nanocomposite structures was carried out by MacManus-Driscoll et al., in which LSMO-ZnO (lanthanum strontium manganite - zinc oxide) and BFO-SmO (bismuth ferrite – samarium oxide) composites were fabricated,[103] among other mixed oxide nanocomposites.[104-106]

A study of growing these self-assembled structures on different substrate planes was carried out with CFO-PT (cobalt ferrite – lead titanate) multiferroics on strontium titanate (STO) substrates of (001) and (110) orientations.[107] The resulting morphology of the nanorods was dependant on the STO substrate orientation, which was rationalized through a

thermodynamic theory based on the ferroelastic anisotropy in the two different systems. A year later this investigation was repeated in a CFO-BFO composite thin films.[108] The group explicitly observed that (001) substrates caused the spontaneous formation of rectangular CFO nanopillars in a BFO matrix, whereas (111) substrates encouraged triangular-shaped BFO nanopillars in a matrix of CFO. This was repeated across a series of spinel-perovskite volume ratios, yielding the same result. This was the first case of the spinel acting as the host matrix, but was later observed in BTO-CFO and BFO-NFO composites by the same group. It was believed to be the result of different nucleation mechanisms in the two crystal structures, where specific substrate orientations encourage one form of nucleation over the other. In the case where neither nucleation mechanism was favoured, it was shown that an intertwined two-phase composite could be formed. In contradiction to this, Wan et al. demonstrated how the nanopillars-matrix morphology could be controlled by modifying the volume ratio of the spinel-perovskite targets when growing on substrates of the same orientation, highlighting the inconsistencies in this area of nanostructuring that needs to be addressed in the future.[109]

Using an alternative fabrication method, CFO-PZT nanostructures were made and characterized also.[110] Through a sol-gel and spin coating technique, nanopillars-matrix samples with sound magnetic and electric hysteresis loops were created. These structures also exhibited strong magnetoelectric coupling. The same conclusions were also drawn from PLD grown NFO-PZT composite films – where notably the ferroelectric and magnetic properties measured were comparable with bulk composites.[111] Another technique for fabricating these composites was demonstrated by Ren and Wuttig, in which they crystallised and spinodally decomposed a gel on silicon to form a PZT-NFO nanostructure.[112] Magnetoelectric coupling was also observed in BFO films which were grown as $BiFeO_3$-Fe_2O_3 (iron oxide) nanocomposites, however the properties were overall found to be similar to pure BFO films.[113] Another example of a self-assembling process for ferroelectrics came in 2005 from Liu and co-

workers.[114] Through a combination of hydrothermal synthesis, a chemical suspension, and PLD, an array configuration with a textured layer of lead zirconate titanate (PZT) microcubes was fabricated in liquids. PFM measurements indicated ferroelectric activity through hysteresis curves.

A widely used alternative to 'top-down' FIB processing in recent years has been to grow thin films onto substrates which are covered with porous anodic aluminium oxide (AAO) masks. In this way, an array of nanostructures are epitaxially grown with a fixed lateral dimension. An early notable use of anodic alumina is the work of Masuda and Fukuda to create a matrix of platinum and gold nanoholes.[115] The porous masks were developed by applying a Si (silicon) mould to an Al (aluminium) matrix, which caused an imprint. Once placed in oxalic acid solution under an electric field the textured Al began to grow channels through the matrix, resulting in the porous AAO mask with periodicities of 100, 150 and 200nm.[116] Soon after this, Li et al. carried out a systematic study of different anodizing acid solutions (oxalic, sulfuric, and phosphoric) and were able to create masks with pore periodicities of 50nm.[117] Sun successfully used various methods of creating the initial textured array on the Al surface,[118] however, Choi et al. observed that due to the self-ordering nature of the anodization process, it is possible to create pores with smaller diameters than defined by the imprint textures.[119] This use of these masks for nanostructuring ferroelectrics was championed by M. Alexe et al. in Halle, Germany. After establishing their own methodology of fabricating AAO masks through hard anodization (providing thick masks not previously achievable),[120, 121] the group created lanthanum-doped bismuth titanate 2D nanocolumn arrays and PZT nanoislands through shadow masking during PLD growth procedures.[122, 123] Characterization through PFM revealed that the PZT islands exhibited exotic vortex domain states, similar to the flux-closure quadrant packages discussed earlier in this review.[79] Magnetoelectric coupling was also identified in dot-matrix nanocomposites of CFO-PZT fabricated through AAO masks.[124]

By combining both self-assembly and AAO masking techniques, Evans et al. created capacitor arrays with memory densities of nearly Tb per square inch.[5] Pt nanowires of 20-40nm diameter were deposited through an AAO mask (with a periodicity of 50-100nm) onto silicon. Then a thin film of either BTO or PZT was deposited on top of the nanowires, with top electrodes deposited to complete the array. Despite poor switching in BTO, a remanent polarization of ~50μC/cm^2 was observed in the PZT samples through very lossy hysteresis loops. The work indicates that high density ferroelectric memory structures can be created.

An intriguing application of nanoscaling ferroelectric heterostructures comes in the form of ferroelectric tunnel junctions (FTJs). Note that whilst a number of papers report success in vertical scaling into the nanoscale regime,[125-128] fully integrated examples are very scarce. These structures show a tunnelling electroresistance effect which enables the resistance to be tuned according to the tunnelling barrier between the ferroelectric layer and a scanning probe tip. This effect was observed in PLD grown mixed-phase BFO and a very large retention time was measured due to the pinning of domains in the regions where both T-phase and R-phase existed.[129] A very recent study carried out by Abuwasib and collaborators shows this potential memory storage device in practice, created through PLD and electron-beam lithography.[130] The group created ferroelectric tunnel junctions of Co-BTO-SRO (cobalt - barium titanate - strontium ruthenate) layers with lateral dimensions of 300nm^2, and measured hysteresis loops and characterised the switching behaviour of the integrated capacitors. The devices exhibited a tunnelling electroresistance effect and a polarization retention of longer than 10 hours, which indicates the possibility of using these structures as low-power resistive switching based memory applications.[131] Similar FTJs have been fabricated through electron-beam lithography in Paris[132-134] consisting of gold-cobalt-BTO-LSMO-NGO (barium titanate - lanthanum strontium manganite – neodymium gallate) nanodevices. These devices where developed as ferroelectric memristors, where the resistance was continuously switched across

two orders of magnitude, a feat that was previously unrealised.[135, 136] Also fabricated via an e-beam lithography method, Co-$BiFeO_3$-$Ca_{0.96}Ce_{0.04}MnO_3$ (cobalt - bismuth ferrite – calcium cerium manganese oxide) FTJs, studied by Boyn et al., showed excellent memory retention (with states predicted to be stable for 10 years) and a resistance endurance of $4x10^6$ cycles. In a systematic investigation of the effect of different top electrode materials in FTJs by the same group of scientists, it was discovered that an increased work function caused an increase in the metal-to-ferroelectric tunnelling barrier.[137] Accompanying this larger barrier, a large internal electric field was identified which could potentially lead to destructive switching voltages. This study highlighted the tuning capabilities of FTJs through material selection, and has paved the way for further investigations which will provide a greater understanding of these promising nanodevices.

6. Conclusion

From the discussion so far, it is clear that the focused ion beam microscope is definitely a mixed blessing when used to machine and pattern ferroelectric materials. On the down-side, the relatively high energies of the incident ions always raise the possibility of damage and ion implantation. As a result, distinct strategies have to be developed which can either minimise the damage in the first place (by progressively lowering the ion accelerating voltages as milling progresses, or by protecting the sample of interest with sacrificial caps or coatings),[38, 41-43] or recover the damage after the milling phase is complete (by combinations of thermal annealing, chemical cleaning and additional low energy polishing).[34-37, 44-49, 51, 52] The problem is that each system will react differently to the FIB milling and will require different damage-recovery protocols; hence distinct processing methods have to be developed for every new ferroelectric material. This is time-consuming and success is not guaranteed: damage-free BaTiO3 nanostructures have been made,[37] but investigations into FIB-patterned KTP by Whyte and co-workers[95-97] were performed on lamellae in which an amorphous surface layer persisted: in the time available during the PhD programme, thermal annealing conditions were not successfully established to allow recrystallization without sample degradation. In this specific case, PFM imaging of domains and domain walls through the amorphous surface layer was possible (probably because of the relatively low permittivity of the KTP) and so domain dynamics could still be mapped effectively.

The serial nature of the FIB milling technique also makes it rather slow, such that it is simply not suitable for volume patterning. Moreover, although the ion optics certainly allow for features to be milled at the tens of nanometres scale in principal (and even sub ten nanometres), the reality is that patterning 3D morphologically distinct, crystallographically intact, objects below length scales of 50nm is very difficult. This can be frustrating if this length scale is simply too large for the specific size-related physics of interest to manifest: for

example, FIB-milled single crystal ferroelectric objects could allow for clear observations of flux-closure domain sets,[69] but the sizes at which surface depolarising fields would force the existence of genuine dipole vortex structures,[70, 71] as predicted using atomistic simulations, could not be achieved.

Having emphasized the problems and frustrations of using the FIB, there is no doubt that it is an incredibly powerful research tool. It allows one-off test structures in the micron to 100nm length scale to be made quickly and, almost uniquely, it allows morphologies to be created in three dimensions which would be almost impossible using any other patterning technique: the archway and nanopillar junction structures made by Blamire and co-workers[138] and the arrow-head KTP lamellae, or lamellae with circular and triangular holes, made by Whyte et al.[97] could not be made in any other way. Even race-track geometries with morphological pinning notches or antinotches, which can be made by optical or e-beam lithography, are quicker and easier to fabricate using FIB.

So what about the future of FIB in the context of machining ferroelectric nanostructures? In the end, this will be limited only by the imagination of the global research community. One obvious area for development, however, is in using the FIB to make ferroelectric nanostructures which mirror those already used in nanomagnetics research. In nanomagnetism, a great deal has been learned about how to control domains in patterned structures: injection of domain walls has been mastered, as has their controlled motion along simple racetracks and around often rather convoluted circuit geometries associated with domain wall logic systems.[139, 140] Domain coupling between distinct race-tracks has been investigated, as has the frustrated coupling response among patterned islands in artificial spin-ice structures. Strategies to optimise domain wall velocities using patterned comb-like structures have been developed, avoiding Walker breakdown.[141] In short, a level of sophistication in using nanostructuring to develop control over domain dynamics has been established in nanomagnetism that is far

beyond the equivalent state-of-the-art in ferroelectrics. Catching up would be motivation in its own right, but ferroelectrics potentially offer something more: it is now clear that ferroelectric domain walls can be conductors[89, 142-149] or perhaps even superconductors[150] when the domains they surround are insulating. If domain wall motion, positioning, injection and annihilation could be controlled to the degree shown in nanomagnetism, then completely new forms of domain wall nanoelectronics[90] could be created in which "now-you-see-it, now-you-don't" conducting channels would entirely dictate device function. New kinds of transistors, for example, have been suggested, where ON and OFF states are determined by the presence or absence of a conducting domain wall channels between source and drain electrodes. The combination of using ferroelectrics in which interesting domain wall functionality exists and FIB patterning to create domain wall device control, building on the accumulated knowledge already there in the nanomagnetics community, could be very powerful indeed.

Acknowledgements

Received:
Revised:
Published online:

[1] M.E. Lines, A.M. Glass, *Principles and Applications of Ferroelectrics and Related Materials,* OUP Oxford, **1977**.

[2] K. Uchino, *Ferroelectric Devices 2nd Edition,* CRC press, **2009**.

[3] P. Muralt, *Journal of Micromechanics and Microengineering*. **2000**, *10*, 2.

[4] C.H. Ahn, T. Tybell, L. Antognazza, K. Char, R.H. Hammond, M.R. Beasley, Ø. Fischer, J.-M. Triscone, *Science*. **1997**, *276*, 5315.

[5] P.R. Evans, X. Zhu, P. Baxter, M. McMillen, J. McPhillips, F.D. Morrison, J.F. Scott, R.J. Pollard, R.M. Bowman, J.M. Gregg, *Nano Lett*. **2007**, *7*, 5.

[6] M. Alexe, J.F. Scott, C. Curran, N.D. Zakharov, D. Hesse, A. Pignolet, *Applied Physics Letters*. **1998**, *73*, 11.

[7] R. Huang, H.C. Ding, W.I. Liang, Y.C. Gao, X.D. Tang, Q. He, C.G. Duan, Z. Zhu, J. Chu, C.A. Fisher, *Advanced Functional Materials*. **2014**, *24*, 6.

[8] V. Nagarajan, S. Prasertchoung, T. Zhao, H. Zheng, J. Ouyang, R. Ramesh, W. Tian, X.Q. Pan, D.M. Kim, C.B. Eom, H. Kohlstedt, R. Waser, *Applied Physics Letters*. **2004**, *84*, 25.

[9] M. Alexe, A. Gruverman, C. Harnagea, N.D. Zakharov, A. Pignolet, D. Hesse, J.F. Scott, *Applied Physics Letters*. **1999**, *75*, 8.

[10] M. Alexe, C. Harnagea, D. Hesse, U. Gösele, *Applied Physics Letters*. **2001**, *79*, 2.

[11] D.G. Schlom, L.-Q. Chen, C.-B. Eom, K.M. Rabe, S.K. Streiffer, J.-M. Triscone, *Annual Review of Materials Research*. **2007**, *37*, 1.

[12] D.G. Schlom, L.-Q. Chen, C.J. Fennie, V. Gopalan, D.A. Muller, X. Pan, R. Ramesh, R. Uecker, *MRS Bulletin*. **2014**, *39*, 02.

[13] F. Johann, A. Morelli, D. Biggemann, M. Arredondo, I. Vrejoiu, *Physical Review B*. **2011**, *84*, 9.

[14] R.J. Zeches, M.D. Rossell, J.X. Zhang, A.J. Hatt, Q. He, C.H. Yang, A. Kumar, C.H. Wang, A. Melville, C. Adamo, G. Sheng, Y.H. Chu, J.F. Ihlefeld, R. Erni, C. Ederer, V. Gopalan, L.Q. Chen, D.G. Schlom, N.A. Spaldin, L.W. Martin, R. Ramesh, *Science*. **2009**, *326*, 5955.

[15] S. Keisuke, U. Alexander, G. Volkmar, R. Heiko, B. Lutz, O. Hideo, K. Toshiyuki, U. Sadao, F. Hiroshi, *Japanese Journal of Applied Physics*. **2006**, *45*, 9S.

[16] Y.H. Chu, L.W. Martin, M.B. Holcomb, M. Gajek, S.J. Han, Q. He, N. Balke, C.H. Yang, D. Lee, W. Hu, Q. Zhan, P.L. Yang, A. Fraile-Rodriguez, A. Scholl, S.X. Wang, R. Ramesh, *Nat Mater*. **2008**, *7*, 6.

[17] T. Zhao, A. Scholl, F. Zavaliche, K. Lee, M. Barry, A. Doran, M.P. Cruz, Y.H. Chu, C. Ederer, N.A. Spaldin, R.R. Das, D.M. Kim, S.H. Baek, C.B. Eom, R. Ramesh, *Nat Mater*. **2006**, *5*, 10.

[18] Y.-H. Chu, L.W. Martin, M.B. Holcomb, R. Ramesh, *Materials Today*. **2007**, *10*, 10.

[19] S.H. Baek, H.W. Jang, C.M. Folkman, Y.L. Li, B. Winchester, J.X. Zhang, Q. He, Y.H. Chu, C.T. Nelson, M.S. Rzchowski, X.Q. Pan, R. Ramesh, L.Q. Chen, C.B. Eom, *Nat Mater*. **2010**, *9*, 4.

[20] M. Liu, O. Obi, J. Lou, Y. Chen, Z. Cai, S. Stoute, M. Espanol, M. Lew, X. Situ, K.S. Ziemer, V.G. Harris, N.X. Sun, *Advanced Functional Materials*. **2009**, *19*, 11.

[21] V.V. Kruglyak, S.O. Demokritov, D. Grundler, *Journal of Physics D: Applied Physics*. **2010**, *43*, 26.

[22] C.A. Volkert, A.M. Minor, *MRS Bulletin*. **2007**, *32*, 05.

[23] R.M. Langford, A.K. Petford-Long, M. Rommeswinkle, S. Egelkamp, *Materials Science and Technology*. **2002**, *18*, 7.

[24] S. Reyntjens, R. Puers, *Journal of Micromechanics and Microengineering*. **2001**, *11*, 4.

[25] J. Melngailis, *Journal of Vacuum Science & Technology B: Microelectronics and Nanometer Structures*. **1987**, *5*, 2.

[26] R.L. Seliger, W.P. Fleming, *Journal of Applied Physics*. **1974**, *45*, 3.

[27] P.M. Nellen, R. Brönnimann, *Measurement Science and Technology*. **2006**, *17*, 5.

[28] J. Gierak, E. Bourhis, G. Faini, G. Patriarche, A. Madouri, R. Jede, L. Bruchhaus, S. Bauerdick, B. Schiedt, A.L. Biance, L. Auvray, *Ultramicroscopy*. **2009**, *109*, 5.

[29] K. Amanuma, T. Kunio, *Japanese Journal of Applied Physics*. **1996**, *35*, 9S.

[30] H. Uchida, N. Soyama, K. Kageyama, K. Ogi, M.C. Scott, J.D. Cuchiaro, L.D. McMillan, C.A.P. De Araujo, *Integrated Ferroelectrics*. **1997**, *18*, 1-4.

[31] J.F. Scott, *Journal of Physics: Condensed Matter*. **2008**, *20*, 2.

[32] M. Alexe, C. Harnagea, D. Hesse, U. Gösele, *Applied physics letters*. **1999**, *75*, 12.

[33] C. Harnagea, A. Pignolet, M. Alexe, D. Hesse, U. Gösele, *Applied Physics A*. **2000**, *70*, 3.

[34] M.M. Saad, R.M. Bowman, J.M. Gregg, *Applied Physics Letters*. **2004**, *84*, 7.

[35] A. Stanishevsky, B. Nagaraj, J. Melngailis, R. Ramesh, L. Khriachtchev, E. McDaniel, *Journal of Applied Physics*. **2002**, *92*, 6.

[36] M.M. Saad, R.R. Bowman, J.M. Gregg, *Integrated Ferroelectrics*. **2004**, *61*, 1.

[37] A. Schilling, T. Adams, R.M. Bowman, J.M. Gregg, *Nanotechnology*. **2007**, *18*, 3.

[38] M. Hambe, S. Wicks, J.M. Gregg, V. Nagarajan, *Nanotechnology*. **2008**, *19*, 17.

[39] K. Torii, K. Shoji, H. Kawakami, T. Kumihashi, T. Itoga, N. Yokoyama, M. Moniwa, T. Kaga, Y. Fujisaki, *Electrical Engineering in Japan*. **1997**, *121*, 1.

[40] I. Vrejoiu, A. Morelli, D. Biggemann, E. Pippel, *Nano Reviews*. **2011**, *2*,

[41] A. Morelli, F. Johann, N. Schammelt, D. McGrouther, I. Vrejoiu, *Journal of Applied Physics*. **2013**, *113*, 15.

[42] A. Morelli, F. Johann, N. Schammelt, I. Vrejoiu, *Nanotechnology*. **2011**, *22*, 26.

[43] F. Johann, A. Morelli, I. Vrejoiu, *Applied Physics Letters*. **2011**, *99*, 8.

[44] L.J. Sinnamon, M.M. Saad, R.M. Bowman, J.M. Gregg, *Applied Physics Letters*. **2002**, *81*, 4.

[45] M.M. Saad, P. Baxter, R.M. Bowman, J.M. Gregg, F.D. Morrison, J.F. Scott, *Journal of Physics: Condensed Matter*. **2004**, *16*, 41.

[46] A. Lookman, R.M. Bowman, J.M. Gregg, J. Kut, S. Rios, M. Dawber, A. Ruediger, J.F. Scott, *Journal of Applied Physics*. **2004**, *96*, 1.

[47] T.M. Shaw, Z. Suo, M. Huang, E. Liniger, R.B. Laibowitz, J.D. Baniecki, *Applied Physics Letters*. **1999**, *75*, 14.

[48] C.B. Parker, J.-P. Maria, A.I. Kingon, *Applied Physics Letters*. **2002**, *81*, 2.

[49] L.W. Chang, M. McMillen, F.D. Morrison, J.F. Scott, J.M. Gregg, *Applied Physics Letters*. **2008**, *93*, 13.

[50] M. Stengel, D. Vanderbilt, N.A. Spaldin, *Nat Mater*. **2009**, *8*, 5.

[51] L.W. Chang, M. Alexe, J.F. Scott, J.M. Gregg, *Adv Mater*. **2009**, *21*, 48.

[52] D. Rémiens, R.H. Liang, C. Soyer, D. Deresmes, D. Troadec, S. Quignon, A. Da Costa, R. Desfeux, *Journal of Applied Physics*. **2010**, *108*, 4.

[53] S. Hong, J.A. Klug, M. Park, A. Imre, M.J. Bedzyk, K. No, A. Petford-Long, O. Auciello, *Journal of Applied Physics*. **2009**, *105*, 6.

[54] J.A. Klug, M.V. Holt, R.N. Premnath, A. Joshi-Imre, S. Hong, R.S. Katiyar, M.J. Bedzyk, O. Auciello, *Applied Physics Letters*. **2011**, *99*, 5.

[55] R. Nath, S. Hong, J.A. Klug, A. Imre, M.J. Bedzyk, R.S. Katiyar, O. Auciello, *Applied Physics Letters*. **2010**, *96*, 16.

[56] A. Stanishevsky, *Journal of Vacuum Science & Technology B: Microelectronics and Nanometer Structures*. **1998**, *16*, 6.

[57] C.S. Ganpule, A. Stanishevsky, Q. Su, S. Aggarwal, J. Melngailis, E. Williams, R. Ramesh, *Applied Physics Letters*. **1999**, *75*, 3.

[58] C.S. Ganpule, A. Stanishevsky, S. Aggarwal, J. Melngailis, E. Williams, R. Ramesh, V. Joshi, C. Paz de Araujo, *Applied Physics Letters*. **1999**, *75*, 24.

[59] S. Bühlmann, B. Dwir, J. Baborowski, P. Muralt, *Applied Physics Letters*. **2002**, *80*, 17.

[60] V. Nagarajan, A. Stanishevsky, L. Chen, T. Zhao, B.-T. Liu, J. Melngailis, A. Roytburd, R. Ramesh, J. Finder, Z. Yu, *Applied physics letters*. **2002**, *81*, 22.

[61] V. Nagarajan, A. Roytburd, R. Ramesh, in *Nanoscale Piezoelectric Phenomena in Epitaxial PZT Thin Films*, Vol. (Eds: M. Alexe and A. Gruverman), Springer, Berlin, **2004**.

[62] A. Schilling, T.B. Adams, R.M. Bowman, J.M. Gregg, G. Catalan, J.F. Scott, *Physical Review B*. **2006**, *74*, 2.

[63] C. Kittel, *Physical Review*. **1946**, *70*, 11-12.
[64] C. Kittel, *Reviews of Modern Physics*. **1949**, *21*, 4.
[65] T. Mitsui, J. Furuichi, *Physical Review*. **1953**, *90*, 2.
[66] A.L. Roytburd, *physica status solidi (a)*. **1976**, *37*, 1.
[67] A. Schilling, R.M. Bowman, J.M. Gregg, G. Catalan, J.F. Scott, *Applied Physics Letters*. **2006**, *89*, 21.
[68] A. Schilling, R.M. Bowman, G. Catalan, J.F. Scott, J.M. Gregg, *Nano Letters*. **2007**, *7*, 12.
[69] A. Schilling, D. Byrne, G. Catalan, K.G. Webber, Y.A. Genenko, G.S. Wu, J.F. Scott, J.M. Gregg, *Nano Lett*. **2009**, *9*, 9.
[70] R. Ahluwalia, N. Ng, A. Schilling, R.G. McQuaid, D.M. Evans, J.M. Gregg, D.J. Srolovitz, J.F. Scott, *Phys Rev Lett*. **2013**, *111*, 16.
[71] L. McGilly, D. Byrne, C. Harnagea, A. Schilling, J.M. Gregg, *Journal of Materials Science*. **2009**, *44*, 19.
[72] L.J. McGilly, A. Schilling, J.M. Gregg, *Nano Lett*. **2010**, *10*, 10.
[73] L.J. McGilly, J.M. Gregg, *Applied Physics Letters*. **2011**, *98*, 13.
[74] A. Schilling, S. Prosandeev, R.G.P. McQuaid, L. Bellaiche, J.F. Scott, J.M. Gregg, *Physical Review B*. **2011**, *84*, 6.
[75] R.G. McQuaid, L.J. McGilly, P. Sharma, A. Gruverman, J.M. Gregg, *Nat Commun*. **2011**, *2*,
[76] R.K. Vasudevan, Y.C. Chen, H.H. Tai, N. Balke, P. Wu, S. Bhattacharya, L.Q. Chen, Y.H. Chu, I.N. Lin, S.V. Kalinin, V. Nagarajan, *ACS Nano*. **2011**, *5*, 2.
[77] Y. Ivry, D.P. Chu, J.F. Scott, C. Durkan, *Physical Review Letters*. **2010**, *104*, 20.
[78] A. Gruverman, D. Wu, H.J. Fan, I. Vrejoiu, M. Alexe, R.J. Harrison, J.F. Scott, *Journal of Physics: Condensed Matter*. **2008**, *20*, 34.
[79] B.J. Rodriguez, X.S. Gao, L.F. Liu, W. Lee, I.I. Naumov, A.M. Bratkovsky, D. Hesse, M. Alexe, *Nano Letters*. **2009**, *9*, 3.
[80] T. Tybell, P. Paruch, T. Giamarchi, J.M. Triscone, *Physical Review Letters*. **2002**, *89*, 9.
[81] R.G. McQuaid, A. Gruverman, J.F. Scott, J.M. Gregg, *Nano Lett*. **2014**, *14*, 8.
[82] L.J. McGilly, J.M. Gregg, *Nano Lett*. **2011**, *11*, 10.
[83] L.W. Chang, V. Nagarajan, J.F. Scott, J.M. Gregg, *Nano Lett*. **2013**, *13*, 6.
[84] C.T. Nelson, B. Winchester, Y. Zhang, S.-J. Kim, A. Melville, C. Adamo, C.M. Folkman, S.-H. Baek, C.-B. Eom, D.G. Schlom, L.-Q. Chen, X. Pan, *Nano Letters*. **2011**, *11*, 2.
[85] C.L. Jia, K.W. Urban, M. Alexe, D. Hesse, I. Vrejoiu, *Science*. **2011**, *331*, 6023.
[86] L.W. Chang, V. Nagarajan, M.B. Okatan, J.M. Gregg, *Journal of Applied Physics*. **2014**, *116*, 6.
[87] Y.L. Tang, Y.L. Zhu, X.L. Ma, A.Y. Borisevich, A.N. Morozovska, E.A. Eliseev, W.Y. Wang, Y.J. Wang, Y.B. Xu, Z.D. Zhang, S.J. Pennycook, *Science*. **2015**,
[88] V. Nagarajan, A. Roytburd, A. Stanishevsky, S. Prasertchoung, T. Zhao, L. Chen, J. Melngailis, O. Auciello, R. Ramesh, *Nat Mater*. **2003**, *2*, 1.
[89] J. Seidel, L.W. Martin, Q. He, Q. Zhan, Y.H. Chu, A. Rother, M.E. Hawkridge, P. Maksymovych, P. Yu, M. Gajek, N. Balke, S.V. Kalinin, S. Gemming, F. Wang, G. Catalan, J.F. Scott, N.A. Spaldin, J. Orenstein, R. Ramesh, *Nat Mater*. **2009**, *8*, 3.
[90] G. Catalan, J. Seidel, R. Ramesh, J.F. Scott, *Reviews of Modern Physics*. **2012**, *84*, 1.
[91] M. McMillen, R.G.P. McQuaid, S.C. Haire, C.D. McLaughlin, L.W. Chang, A. Schilling, J.M. Gregg, *Applied Physics Letters*. **2010**, *96*, 4.
[92] R.G. McQuaid, L.W. Chang, J.M. Gregg, *Nano Lett*. **2010**, *10*, 9.
[93] R.G. McQuaid, M. McMillen, L.W. Chang, A. Gruverman, J.M. Gregg, *J Phys Condens Matter*. **2012**, *24*, 2.
[94] P. Sharma, R.G. McQuaid, L.J. McGilly, J.M. Gregg, A. Gruverman, *Adv Mater*. **2013**, *25*, 9.
[95] J.R. Whyte, R.G. McQuaid, P. Sharma, C. Canalias, J.F. Scott, A. Gruverman, J.M. Gregg, *Adv Mater*. **2014**, *26*, 2.
[96] J.R. Whyte, R.G.P. McQuaid, C.M. Ashcroft, J.F. Einsle, C. Canalias, A. Gruverman, J.M. Gregg, *Journal of Applied Physics*. **2014**, *116*, 6.

[97] J.R. Whyte, J.M. Gregg, *Nat Commun*. **2015**, *6*,
[98] L.W. Martin, S.P. Crane, Y.H. Chu, M.B. Holcomb, M. Gajek, M. Huijben, C.H. Yang, N. Balke, R. Ramesh, *Journal of Physics: Condensed Matter*. **2008**, *20*, 43.
[99] H. Zheng, J. Wang, S.E. Lofland, Z. Ma, L. Mohaddes-Ardabili, T. Zhao, L. Salamanca-Riba, S.R. Shinde, S.B. Ogale, F. Bai, D. Viehland, Y. Jia, D.G. Schlom, M. Wuttig, A. Roytburd, R. Ramesh, *Science*. **2004**, *303*, 5658.
[100] F. Zavaliche, H. Zheng, L. Mohaddes-Ardabili, S.Y. Yang, Q. Zhan, P. Shafer, E. Reilly, R. Chopdekar, Y. Jia, P. Wright, D.G. Schlom, Y. Suzuki, R. Ramesh, *Nano Letters*. **2005**, *5*, 9.
[101] F. Zavaliche, T. Zhao, H. Zheng, F. Straub, M.P. Cruz, P.L. Yang, D. Hao, R. Ramesh, *Nano Letters*. **2007**, *7*, 6.
[102] Q. Zhan, R. Yu, S.P. Crane, H. Zheng, C. Kisielowski, R. Ramesh, *Applied Physics Letters*. **2006**, *89*, 17.
[103] J.L. MacManus-Driscoll, P. Zerrer, H. Wang, H. Yang, J. Yoon, A. Fouchet, R. Yu, M.G. Blamire, Q. Jia, *Nat Mater*. **2008**, *7*, 4.
[104] W. Zhang, R. Ramesh, J.L. MacManus-Driscoll, H. Wang, *MRS Bulletin*. **2015**, *40*, 09.
[105] A. Chen, Z. Bi, Q. Jia, J.L. MacManus-Driscoll, H. Wang, *Acta Materialia*. **2013**, *61*, 8.
[106] W. Zhang, A. Chen, Z. Bi, Q. Jia, J.L. MacManus-Driscoll, H. Wang, *Current Opinion in Solid State and Materials Science*. **2014**, *18*, 1.
[107] J. Li, I. Levin, J. Slutsker, V. Provenzano, P.K. Schenck, R. Ramesh, J. Ouyang, A.L. Roytburd, *Applied Physics Letters*. **2005**, *87*, 7.
[108] H. Zheng, Q. Zhan, F. Zavaliche, M. Sherburne, F. Straub, M.P. Cruz, L.Q. Chen, U. Dahmen, R. Ramesh, *Nano Lett*. **2006**, *6*, 7.
[109] J.G. Wan, Y. Weng, Y. Wu, Z. Li, J.M. Liu, G. Wang, *Nanotechnology*. **2007**, *18*, 46.
[110] J.G. Wan, X.W. Wang, Y.J. Wu, M. Zeng, Y. Wang, H. Jiang, W.Q. Zhou, G.H. Wang, J.-M. Liu, *Applied Physics Letters*. **2005**, *86*, 12.
[111] H. Ryu, P. Murugavel, J.H. Lee, S.C. Chae, T.W. Noh, Y.S. Oh, H.J. Kim, K.H. Kim, J.H. Jang, M. Kim, C. Bae, J.-G. Park, *Applied Physics Letters*. **2006**, *89*, 10.
[112] S. Ren, M. Wuttig, *Applied Physics Letters*. **2007**, *91*, 8.
[113] M. Murakami, S. Fujino, S.-H. Lim, L.G. Salamanca-Riba, M. Wuttig, I. Takeuchi, B. Varughese, H. Sugaya, T. Hasegawa, S.E. Lofland, *Applied Physics Letters*. **2006**, *88*, 11.
[114] X. Liu, E.F. McCandlish, L.E. McCandlish, K. Mikulka-Bolen, R. Ramesh, F. Cosandey, G.A. Rossetti, R.E. Riman, *Langmuir*. **2005**, *21*, 8.
[115] H. Masuda, K. Fukuda, *Science*. **1995**, *268*, 5216.
[116] H. Masuda, H. Yamada, M. Satoh, H. Asoh, M. Nakao, T. Tamamura, *Applied Physics Letters*. **1997**, *71*, 19.
[117] A.P. Li, F. Müller, A. Birner, K. Nielsch, U. Gösele, *Journal of Applied Physics*. **1998**, *84*, 11.
[118] Z. Sun, H.K. Kim, *Applied Physics Letters*. **2002**, *81*, 18.
[119] J. Choi, K. Nielsch, M. Reiche, R.B. Wehrspohn, U. Gösele, *Journal of Vacuum Science & Technology B*. **2003**, *21*, 2.
[120] W. Lee, M. Alexe, K. Nielsch, U. Gösele, *Chemistry of Materials*. **2005**, *17*, 13.
[121] W. Lee, R. Ji, U. Gosele, K. Nielsch, *Nat Mater*. **2006**, *5*, 9.
[122] S.K. Lee, W. Lee, M. Alexe, K. Nielsch, D. Hesse, U. Gösele, *Applied Physics Letters*. **2005**, *86*, 15.
[123] W. Lee, H. Han, A. Lotnyk, M.A. Schubert, S. Senz, M. Alexe, D. Hesse, S. Baik, U. Gosele, *Nat Nano*. **2008**, *3*, 7.
[124] X. Gao, B.J. Rodriguez, L. Liu, B. Birajdar, D. Pantel, M. Ziese, M. Alexe, D. Hesse, *ACS Nano*. **2010**, *4*, 2.
[125] Z. Wen, L. You, J. Wang, A. Li, D. Wu, *Applied Physics Letters*. **2013**, *103*, 13.
[126] A. Sokolov, O. Bak, H. Lu, S. Li, E.Y. Tsymbal, A. Gruverman, *Nanotechnology*. **2015**, *26*, 30.
[127] A. Gruverman, D. Wu, H. Lu, Y. Wang, H.W. Jang, C.M. Folkman, M.Y. Zhuravlev, D. Felker, M. Rzchowski, C.B. Eom, E.Y. Tsymbal, *Nano Letters*. **2009**, *9*, 10.

[128] A.V. Singh, M. Althammer, K. Rott, G. Reiss, A. Gupta, *Applied Physics Letters*. **2015**, *107*, 12.
[129] Y.C. Huang, Y. Liu, Y.T. Lin, H.J. Liu, Q. He, J. Li, Y.C. Chen, Y.H. Chu, *Advanced Materials*. **2014**, *26*, 36.
[130] M. Abuwasib, H. Lu, T. Li, P. Buragohain, H. Lee, C.-B. Eom, A. Gruverman, U. Singisetti, *Applied Physics Letters*. **2016**, *108*, 15.
[131] J.A. Hutchby, R. Cavin, V. Zhirnov, J.E. Brewer, G. Bourianoff, *Computer*. **2008**, *41*, 5.
[132] A. Chanthbouala, A. Crassous, V. Garcia, K. Bouzehouane, S. Fusil, X. Moya, J. Allibe, B. Dlubak, J. Grollier, S. Xavier, C. Deranlot, A. Moshar, R. Proksch, N.D. Mathur, M. Bibes, A. Barthelemy, *Nat Nano*. **2012**, *7*, 2.
[133] V. Garcia, S. Fusil, K. Bouzehouane, S. Enouz-Vedrenne, N.D. Mathur, A. Barthelemy, M. Bibes, *Nature*. **2009**, *460*, 7251.
[134] A. Chanthbouala, V. Garcia, R.O. Cherifi, K. Bouzehouane, S. Fusil, X. Moya, S. Xavier, H. Yamada, C. Deranlot, N.D. Mathur, M. Bibes, A. Barthélémy, J. Grollier, *Nat Mater*. **2012**, *11*, 10.
[135] A. Chanthbouala, R. Matsumoto, J. Grollier, V. Cros, A. Anane, A. Fert, A.V. Khvalkovskiy, K.A. Zvezdin, K. Nishimura, Y. Nagamine, H. Maehara, K. Tsunekawa, A. Fukushima, S. Yuasa, *Nat Phys*. **2011**, *7*, 8.
[136] X. Wang, Y. Chen, H. Xi, H. Li, D. Dimitrov, *IEEE Electron Device Letters*. **2009**, *30*, 3.
[137] S. Boyn, V. Garcia, S. Fusil, C. Carrétéro, K. Garcia, S. Xavier, S. Collin, C. Deranlot, M. Bibes, A. Barthélémy, *APL Mater.* **2015**, *3*, 6.
[138] M. Blamire, A. Aziz, J. Robinson, *Philosophical Transactions of the Royal Society of London A: Mathematical, Physical and Engineering Sciences*. **2011**, *369*, 1948.
[139] D.A. Allwood, G. Xiong, C. Faulkner, D. Atkinson, D. Petit, R. Cowburn, *Science*. **2005**, *309*, 5741.
[140] S.S.P. Parkin, M. Hayashi, L. Thomas, *Science*. **2008**, *320*, 5873.
[141] E.R. Lewis, D. Petit, L. O'Brien, A. Fernandez-Pacheco, J. Sampaio, A.V. Jausovec, H.T. Zeng, D.E. Read, R.P. Cowburn, *Nat Mater*. **2010**, *9*, 12.
[142] J. Guyonnet, I. Gaponenko, S. Gariglio, P. Paruch, *Advanced Materials*. **2011**, *23*, 45.
[143] P. Maksymovych, J. Seidel, Y.H. Chu, P. Wu, A.P. Baddorf, L.Q. Chen, S.V. Kalinin, R. Ramesh, *Nano Lett*. **2011**, *11*, 5.
[144] M. Schröder, A. Haußmann, A. Thiessen, E. Soergel, T. Woike, L.M. Eng, *Advanced Functional Materials*. **2012**, *22*, 18.
[145] D. Meier, J. Seidel, A. Cano, K. Delaney, Y. Kumagai, M. Mostovoy, N.A. Spaldin, R. Ramesh, M. Fiebig, *Nat Mater*. **2012**, *11*, 4.
[146] T. Sluka, A.K. Tagantsev, P. Bednyakov, N. Setter, *Nat Commun*. **2013**, *4*,
[147] Y.S. Oh, X. Luo, F.-T. Huang, Y. Wang, S.-W. Cheong, *Nat Mater*. **2015**, *14*, 4.
[148] Y. Kim, M. Alexe, E.K.H. Salje, *Applied Physics Letters*. **2010**, *96*, 3.
[149] R.K. Vasudevan, A.N. Morozovska, E.A. Eliseev, J. Britson, J.C. Yang, Y.H. Chu, P. Maksymovych, L.Q. Chen, V. Nagarajan, S.V. Kalinin, *Nano Lett*. **2012**, *12*, 11.
[150] A. Alison, K.H.S. Ekhard, *Journal of Physics: Condensed Matter*. **1998**, *10*, 22.

List of Figures

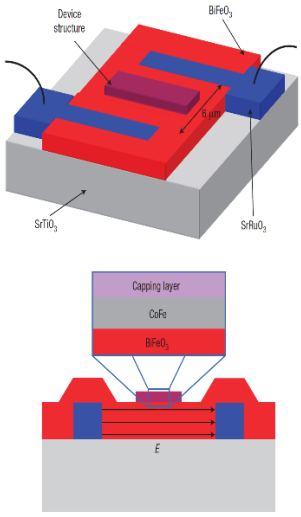

Figure 1. Novel ferromagnetic cobalt-iron (CoFe)/multiferroic bismuth ferrite (BFO) heterostructure devices partially fabricated via focused-ion-beam (FIB). Enabled electric field control of ferromagnetic switching. Established a method of studying magnetoelectric coupling through such fabrication techniques. Reproduced with permission.[16] (Copyright Year, Publisher)

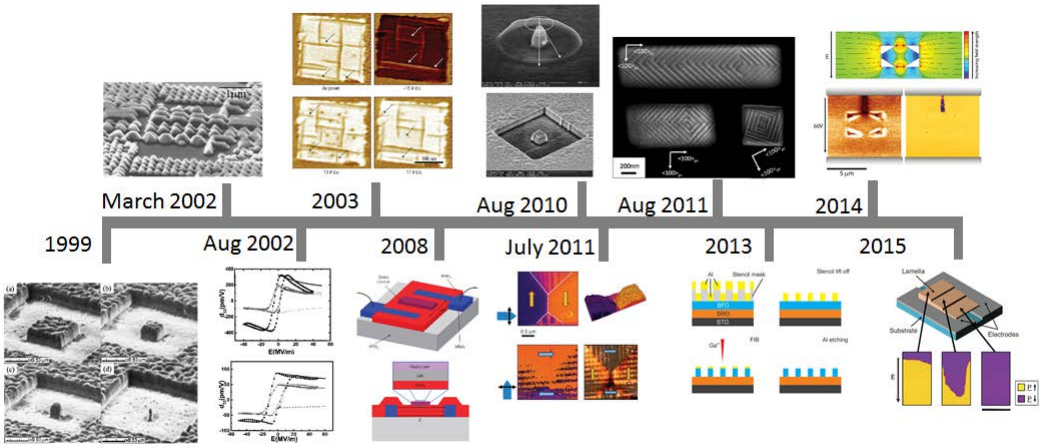

Figure 2. Timeline of significant results from FIB processing of ferroelectrics. Adapted from [16, 41, 52, 58-60, 74, 75, 88, 95, 97]. (Copyright Year, Publisher)

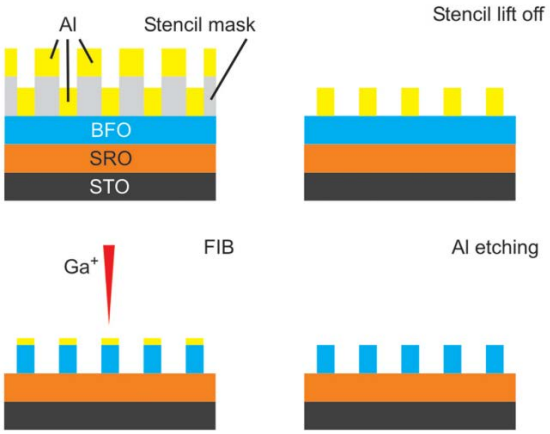

Figure 3. Schematics describing the fabrication of BFO nanoislands, including Al deposition through a stencil mask, the removal of the mask, the ion milling, and the chemical etch to remove any remaining Al. Reproduced with permission.[41] (Copyright Year, Publisher)

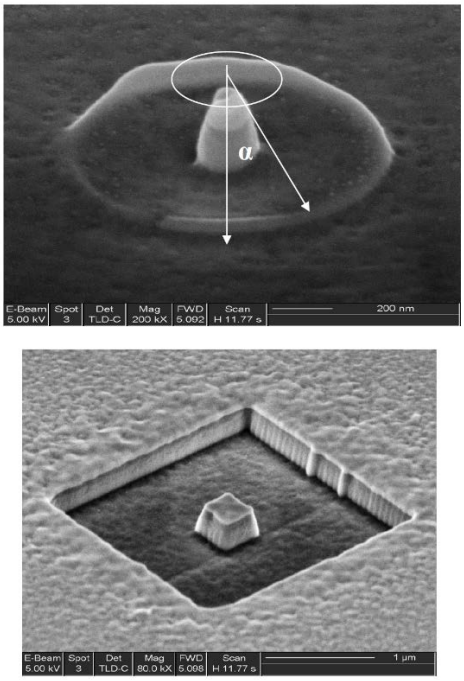

Figure 4. SEM image of a 50nm diameter PZT island milled from an amorphous film layer (top), and a 250nm^2 island milled from a crystalline PZT thin film (bottom). Reproduced with permission.[52] (Copyright Year, Publisher)

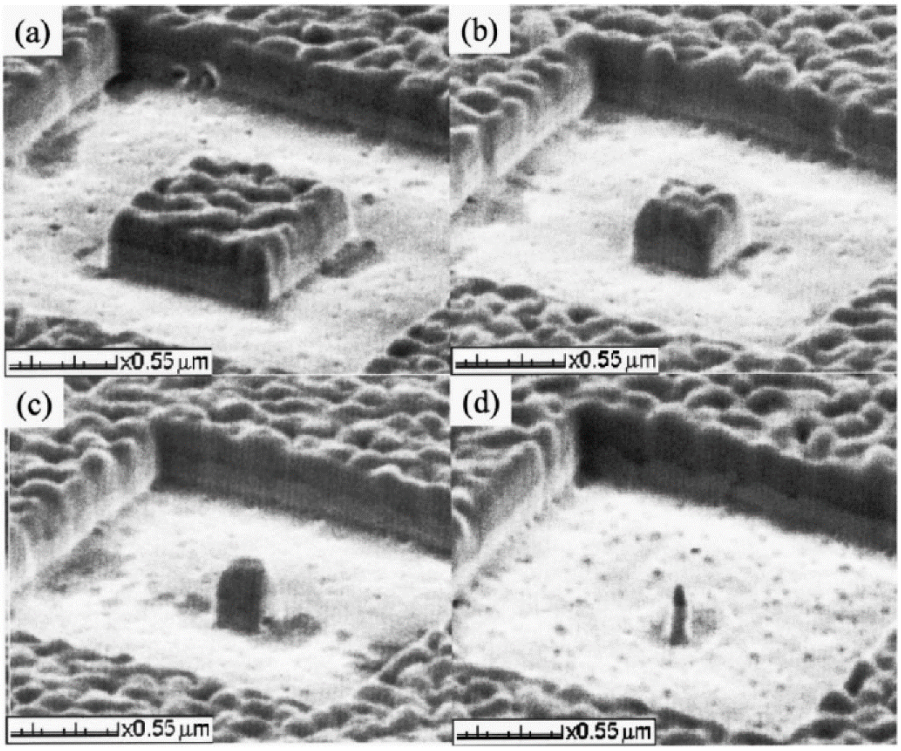

Figure 5. Scanning ion images of SBT nanocapacitors with dimensions of (a)-(c) 1μm^2 to 0.25μm^2 and (d) 70nm^2. Reproduced with permission.[58] (Copyright Year, Publisher)

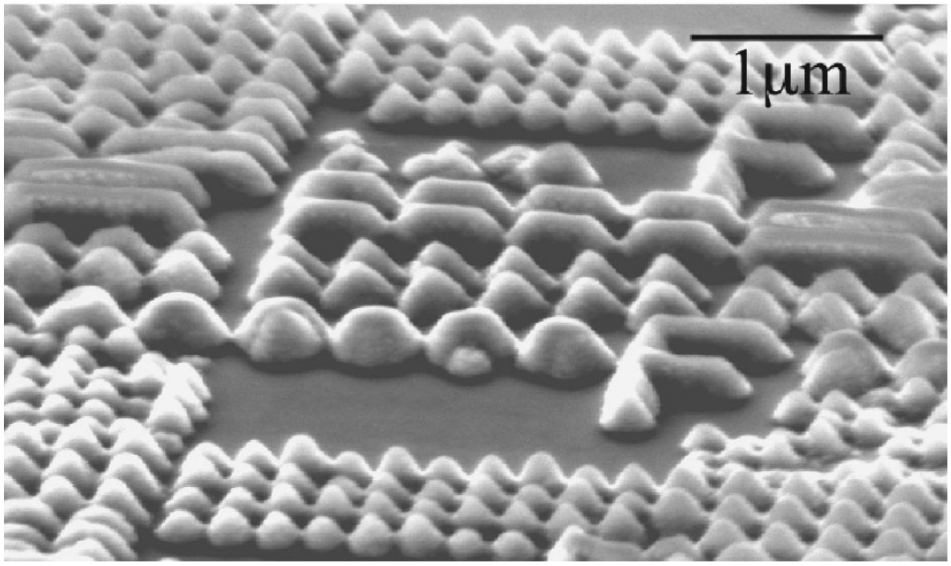

Figure 6. SEM image of PZT capacitors of lateral sizes in the range 100nm to 1μm. Reproduced with permission.[59] (Copyright Year, Publisher)

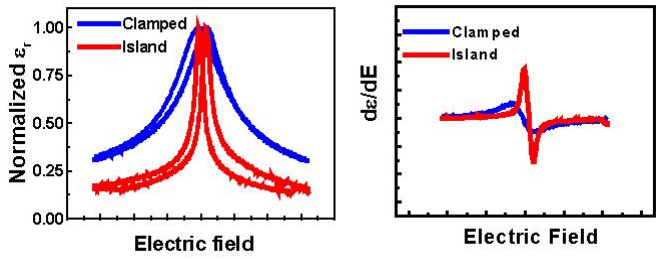

Figure 7. Normalized dielectric response, and first derivitative of dielectric response, of hard ferroelectric PZT with applied external electric field. The sharper response is clear in the unclamped PZT island. Reproduced with permission.[61] (Copyright Year, Publisher)

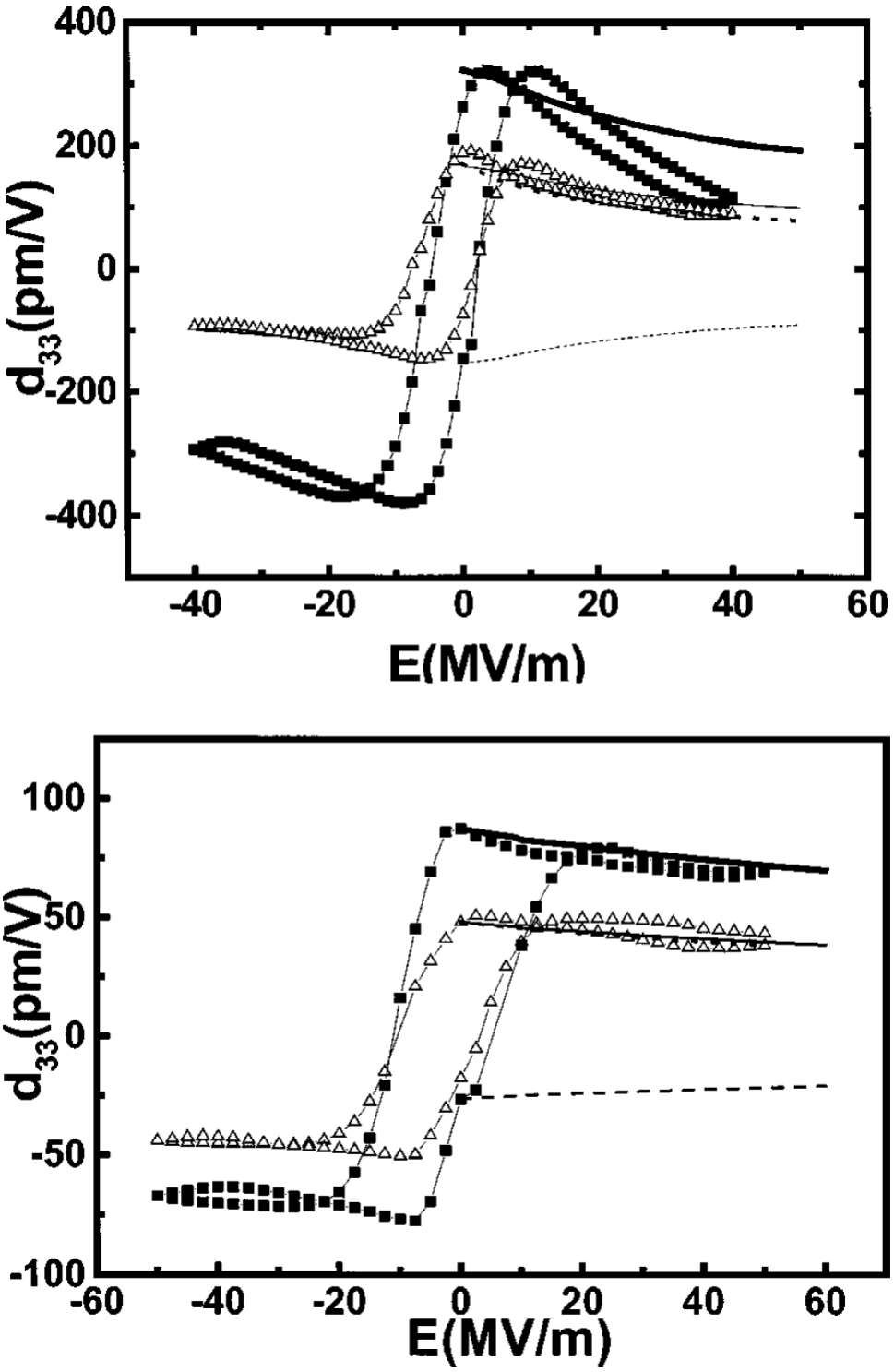

Figure 8. Hysteresis loops for soft (top) and hard (bottom) PZT ferroelectric capacitors. Triangles are measurements from bulk compositions, squares are milled capacitors, solid black lines are predicted behaviour for milled capacitors, and dashed lines are theoretical predictions. Reproduced with permission.[60] (Copyright Year, Publisher)

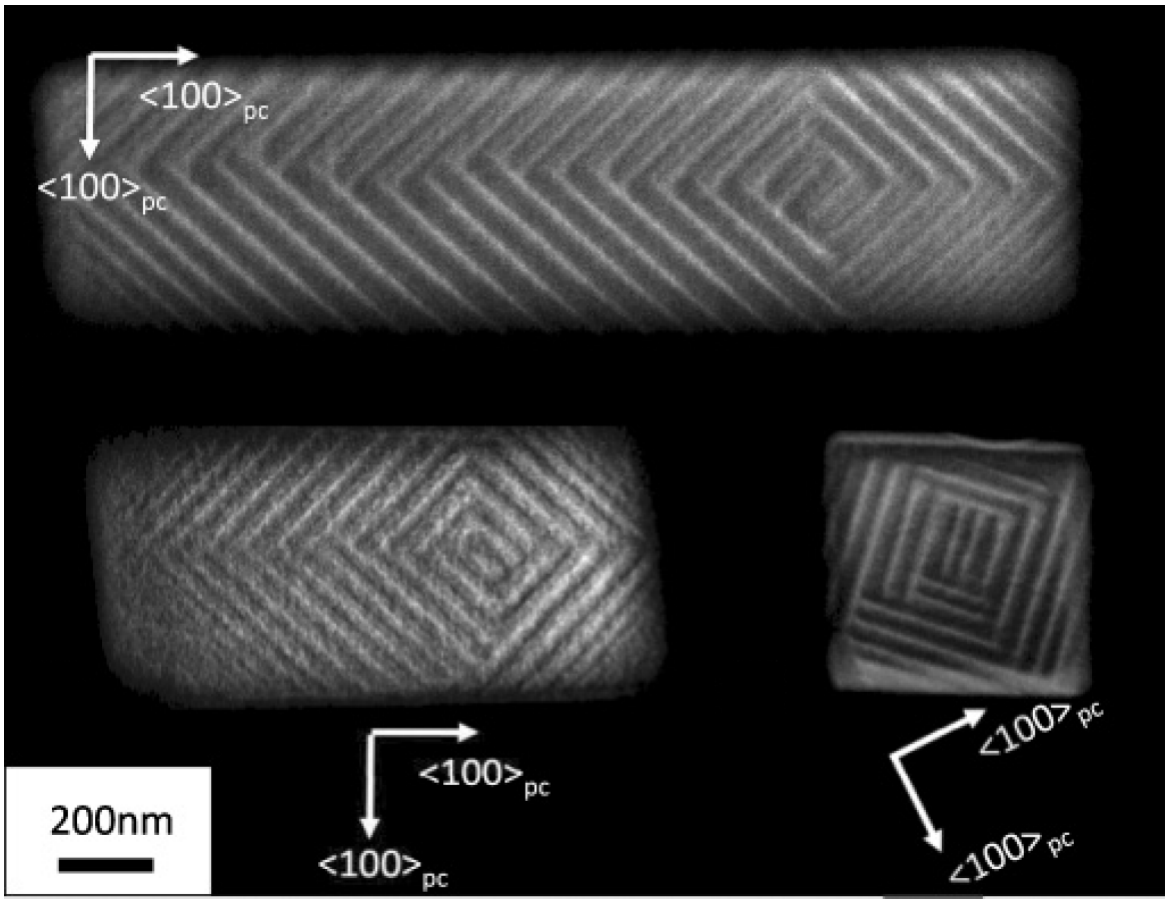

Figure 9. TEM imaging of BTO nanodots and their self-assembling exotic domain structures. The centre-point of the domain quadrant packets migrates towards the side wall as the aspect ratio of the lateral dimensions is changed; this was modelled as a Landau free energy function with 'degree of off-centring' as the order parameter. Reproduced with permission.[74] (Copyright Year, Publisher)

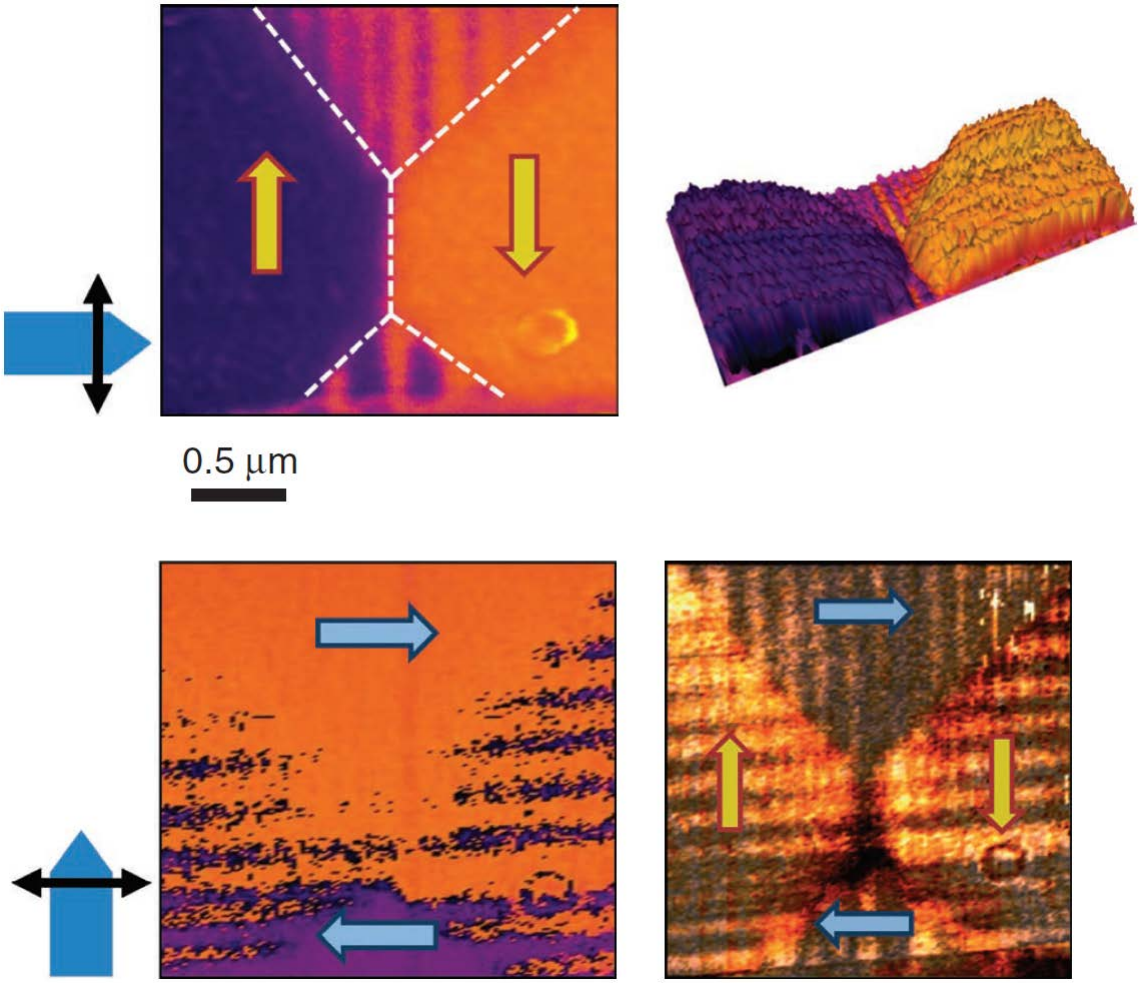

Figure 10. Vector PFM domain mapping of BTO lamella, including orthogonal lateral domain maps (top and bottom left), and a three-dimensional representation of phase (top right) and an overall polarization configuration map from the vector analysis (bottom right). Reproduced with permission.[75] (Copyright Year, Publisher)

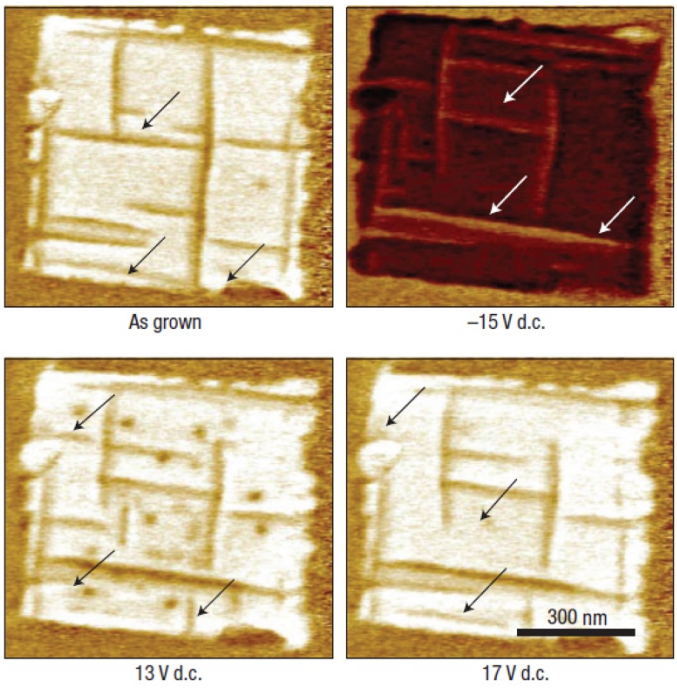

Figure 11. PFM domain mapping of a PZT nanoisland imaged under different applied bias from the scanning tip, highlighting the motion of ferroelastic domain walls across the nanostructure. Reproduced with permission.[88] (Copyright Year, Publisher)

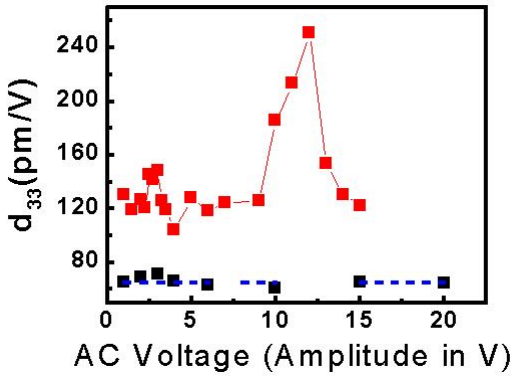

Figure 12. d_{33} across a range of applied voltages, where the red points represent the island and the blue represent the clamped film. The coercive field for 90° domain walls is approximately 12V. Reproduced with permission.[61] (Copyright Year, Publisher)

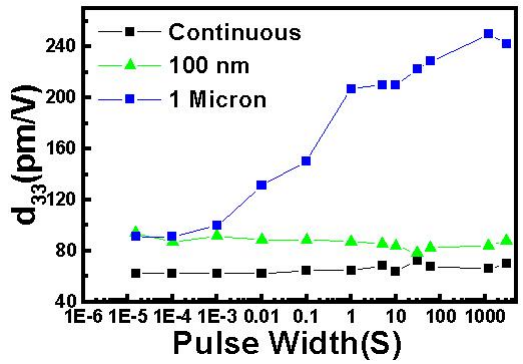

Figure 13. The dielectric response of a clamped PZT film, a 100nm thick unclamped island and a 1µm thick unclamped island. The 1µm thick island geometry, containing the only 90° domain walls across the three samples, is the only one to exhibit a pulse width dependance. Reproduced with permission.[61] (Copyright Year, Publisher)

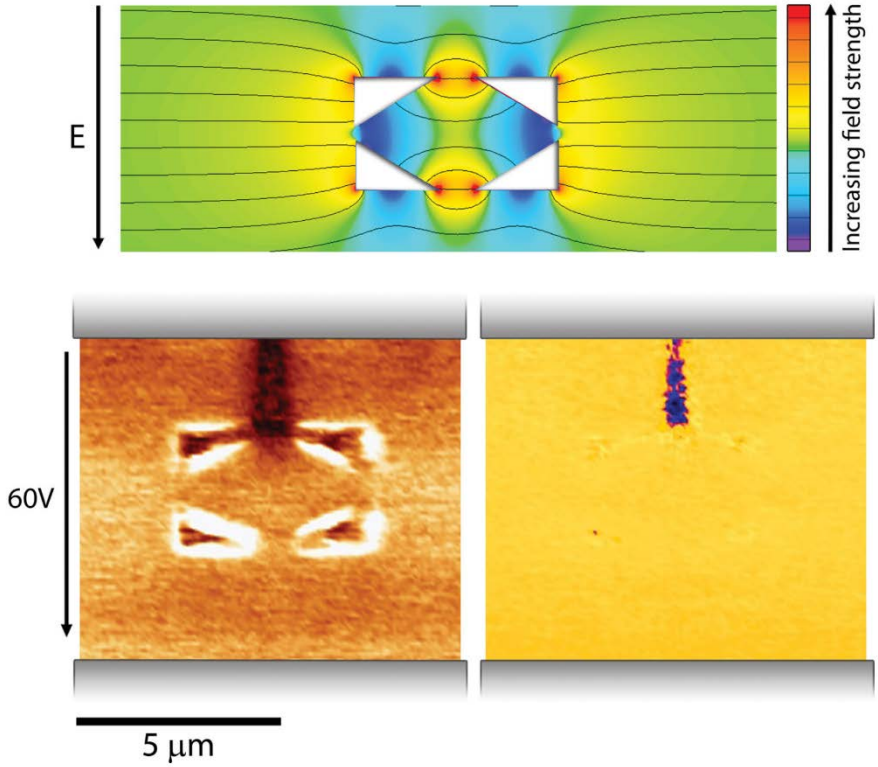

Figure 14. Electric field finite element simulation of a KTP lamella with milled shape defects present (top). PFM imaging of a domain wall nucleation event occurring at the milled defects (amplitude on left, phase on right). Reproduced with permission.[95] (Copyright Year, Publisher)

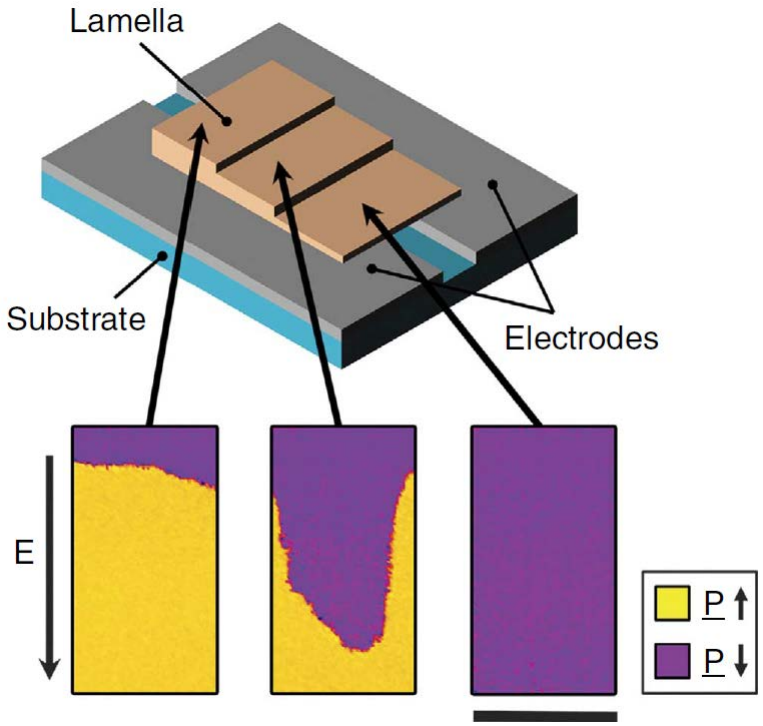

Figure 15. Schematic representation of the sawtooth lamellar capacitor structure made from milled KTP, and PFM scans of each of the 'terraced' areas of the structure, with decreasing thickness from left to right. This shows how the thinnest area has reverse switched entirely from an initially monodomain state, whereas the thickest area has hardly switched at all. Reproduced with permission.[97] (Copyright Year, Publisher)

((**For Essays, Feature Articles, Progress Reports, and Reviews,** please insert up to three author biographies and photographs here, max. 100 words each))

Author Photograph(s) ((40 mm broad, 50 mm high, gray scale))